Materials Science Forum
ISSN: 1662-9752, Vol. 1062, pp 195-203
doi:10.4028/p-a08hju

Submitted: 2021-10-15
Accepted: 2022-03-07
Online: 2022-05-31

The Development of Monolithic Silicon Carbide Intracortical Neural Interfaces for Long-Term Human Implantation

C. Frewin,[1,a] M. Beygi,[2,b] E. Bernardin,[2,c] C. Feng,[2,3,d] F. La Via[4,e], William Dominguez-Viqueira[5,f] and S.E. Saddow[2,6,g*]

[1]NeuroNexus, LLC, Ann Arbor, MI, USA

[2]Dept. of Electrical Engineering Dept., University of South Florida, Tampa, FL, USA

[3]Dept. of Mechanical Engineering, University of South Florida, Tampa, FL, USA

[4]IMM-CNR, Catania, Sicily, IT

[5] Moffitt Cancer Center, Tampa, FL, USA

[6]Dept. of Medical Engineering, University of South Florida, Tampa, FL, USA

[a]cfrewin@neuronexus.com, [b]beygi.mohamad@gmail.com, [c]evans.bernardin@outlook.com, [d]chenyinfeng@usf.edu, [e]francesco.lavia@imm.cnr.it, [f]William.DominguezViqueira@moffitt.org, [g]saddow@usf.edu

Keywords: Neural Interface, Brain Implants, SiC biomedical, MEMS

Abstract. Silicon Carbide (SiC) has been demonstrated as both a bio- and neuro-compatible wide-band-gap semiconductor with a high thermal conductivity and magnetic susceptibility and may be potentially compatible with human brain tissue. Two single-crystal, solid-state forms of SiC have been used to create monolithic intracortical neural implants (INI) without using physiologically exposed metals or polymers, thus eliminating many known reliability challenges in-vivo through a single, homogenous material. Amorphous SiC (*a*-SiC) was used to insulate 16-channel functional INI and the electrochemical and MRI compatibility (7T) performance were measured. 4H-SiC interfaces were fabricated using homoepitaxy,alternating epitaxial films of n-type and p-type forming an isolating PN junction which prevents substrate leakage current between the 16 adjacent electrodes and traces fabricated which were formed using deep-reactive ion etching (DRIE). 3C-SiC interfaces were fabricated in a similar fashion, but the epitaial conductive layers were grown on on both bulk crystalline (100) silicon and SOI wafers. In both cases a conformal coating of *a*-SiC was used as the top-side insulator and windows opened using RIE to allow electrochemical interaction. Electrochemical charaterization achieved through electrochemcial impedance spectroscopy (EIS) and cyclic voltammetry (CV) indicates performance on par, or exceeding, that of Pt reference electrodes with the same form fit. While magnetic resonance imaging (MRI) is an essential, non-contact method used to investigate issues with the nervous system, the high field MRI (e.g., 3 T and higher) necessary for proper diagnosis can be a safety issue for patients with INI due to inductive coupling between the powerful electromagnetic fields and the implanted device. This results in having to use lower electromagnetic field power (less than 1.5T), and therefore lower resolution, which hinders diagnostic prognosis for these patients. In this work the MRI compliance of epitaxial, monolithic SiC INI was studied. The specific absorption rate (SAR), induced heating, and image artifacts caused by the portion of the implant within a brain tissue phantom located in a 7 T small animal MRI machine were estimated and measured via finite element method (FEM) and Fourier-based simulations. Both the simulation and experimental results revealed that free-standing 3C-SiC films had no observable image artifacts compared to silicon and platinum reference materials inside the MRI at 7 T while FEM simulations predicted an ~30% SAR reduction for 3C-SiC compared to Pt. These initial simulations and experiments indicate a SiC monolithic INI may effectively reduce MRI induced heating and image artifacts in high field MRI.

Introduction

Silicon Carbide (SiC) is a potentially biocompatible semiconductor [1] material that may revolutionize implantable biomedical devices, such as biosensors and neural implants, and could enable many advanced biomedical applications [2]. SiC devices offer higher power densities and lower energy losses, as well as being chemically inert and physically robust, allowing the development of lighter, more compact, and higher efficiency products ideal for long-term in-vivo applications. Applications can range from passive material components, like heart stent coatings and bone implant scaffolds, to more complicated devices, like neurological implants and biosensors. One of the large issues facing the medical device community has been the lack of physiologically acceptable materials which also offer electronic functionality. Most of the current implementations of electrically active biomedical devices use silicon materials technology, which is unfortunately a material only stable in-vivo for acute periods of time, usually measured in months reliably [3, 4, 5, 6]. Biomedical devices designed for permanent, chronic applications, like physiological sensors, brain-machine-interfaces (BMI), and smart structural (bone) or organ implants, require a more robust, reliable material that is not only electrically functional, but is not recognized as a foreign object within the biological system [7]. A physiologically compatible, chronically implantable device designed to interact directly with individual cells has great potential to assist millions of people affected by trauma or disease of the brain and spinal cord as well as individuals who have lost limbs or sensory organs. This kind of device potentially has the effect of not only restoring patient health, but also improving their overall quality of life. Unfortunately, as devices become smaller so they can interact with individual cells, they fail chronically in-vivo which has been attributed to both abiotic and biotic factors. Until now, no known, chronically reliable solution to this device challenge has been found, however, silicon carbide may complement or even replace materials, like silicon, as it has demonstrated excellent performance in multiple animal models as well as chemical and physical evaluations [7]. In particular, 3C-SiC the cubic crystalline polytype of silicon carbide, appears to be an ideal material to meet this challenging application: it has demonstrated evidence of bio- and hemocompatibility; the deposition of this polytype allows for tailored doping profiles as well as integration onto silicon platforms allowing seamless integration of electronics with the implants; it is highly durable and chemically inert, even within harsh, corrosive, and oxidative physiological environment; SiC is also an excellent thermal conductor.

This paper focuses on recent advances in the development of monolithic silicon carbide intracortical neural implants, specifically where only SiC is the only material in contact with the physiological environment. These monolithic 'all-SiC' implants were constructed using SiC as the electrical device material and amorphous SiC (*a*-SiC) as an external insulator [8, 9]. Three different devices are reported: 4H-SiC, 3C-SiC and carbon-electrodes which are sandwiched between a top and bottom layer of *a*-SiC, inevitably to form an ultra-thin (<1μm) implant [10]. Device fabrication and electrochemical characterization are reported for all three device types of devices, with MRI compatibility analysis reported for free-standing 3C-SiC implants [11].

Monolithic SiC Neural Interfaces

Monolithic intracortical neural interfaces (INI) designed to interact directly with individual neurons have made impressive progress towards human utilization in recent years, but still display questionable long-term reliability. In this paper we report on the development and characterization of highly resilient SiC INI. SiC is a physically robust, biocompatible, and chemically inert semiconductor. Two monolithic 'all-SiC' INI are reported here comprised of monocrystalline 4H-SiC and 3C-SiC. Details of each device may be found in the literature as reported by Bernardin *et. Al* [8] and Beygi *et. Al* [9], respectfully. A planar MEA design (Fig. 1(a)) was used to characterize neural probe performance using single-ended electrodes of varying tip diameter (25, 50, 100, 400, and 800 μm), PN diode test structures and double-ended mesa resistors to evaluate electrode resistivity.

4H-SiC Fabrication and Characterization: The device support was micromachined from p-type 4H-SiC, with conductors created from n-type 4H-SiC, simultaneously providing electrical isolation through the resulting pn junction. *a*-SiC was utilized as the top side insulation, preventing shorting of the pn diode by the electrochemical environment. Electrodes were designed with a geometric surface area (GSA) varying from 496 to 500k μm^2. Electrical characterization showed high-performance pn diode behavior, with typical turn-on voltages of ~2.3 V and reverse bias leakage below 1 nA_{rms}. Current leakage between adjacent electrodes was maximally ~7.5 nA_{rms} over a voltage range of −50 V to 50 V. Since the monolithic SiC devices rely on the integration of only robust and highly compatible SiC material, they offer a promising solution to probe delamination and biological rejection often associated with the use of multiple materials used in many current INI devices.

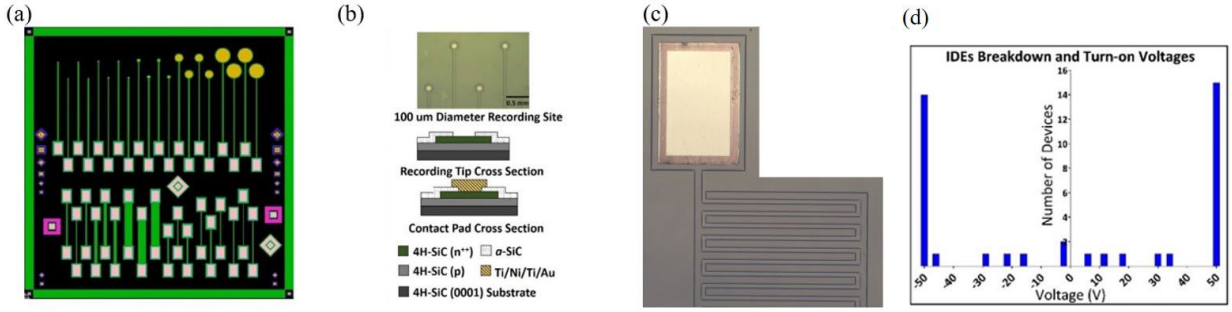

Figure 1: 4H-SiC All-SiC planar device used for electrical and electrochemical testing. (**a**) planar MEA mask with single-ended electrodes (top half) of varying recording tip diameter and test structures (bottom half). (**b**) Optical micrograph of fabricated 100 μm diameter all-SiC single-ended electrodes. (**c**) One end of an all-SiC interdigitated electrode (IDE) showing metal contact pad (top) and portion of two interdigitated 50 μm wide mesas of n^+ on p base layer with a pitch of 25 μm. (d) Histogram of 20 IDE devices from −50 V to +50 V. Of 20 devices, only 2 showed measurable current flow at the p–n diode turn-on voltage (+2.3 V), while 4 IDEs showed current flow between −16 V to −50 V. The remaining 14 continued to block to at least ±50 V.

Electrodes which display semi-metallic charge transport can be fabricated by degenerately doping the SiC epilayer during the growth process. The use of alternate polarity SiC, heavily doped n-type grown on p-type SiC, creates a pn diode, which provides isolation between adjacent electrodes due to the depletion layer that develops at the junction. Amorphous SiC (*a*-SiC) then serves as a conformal, top-side insulating coating to prevent the electrochemical environment from interacting with the pn diode junction or the SiC electrical traces. A high quality 4H-SiC epiwafer was grown and delivered to the USF SiC group by researchers at Linköping University (Linköping, Sweden [8]). Once received all-SiC INI development began with the fabrication of devices on 4H-SiC as illustrated in Fig. 1.

Electrochemical performance was evaluated using electrochemical impedance spectroscopy (EIS) and cyclical voltammetry (CV) in 7.4 pH aerated PBS. Experimental results verified that the n^+ trace length did not significantly affect the overall electrical impedance of the SiC electrodes, a similar effect seen with conventional neural probes metal traces. The results from the EIS measurements are shown in Figure 2(a). The electrode interaction with the electrolyte displayed a nearly purely capacitive characteristic at frequencies less than 10 kHz, as is displayed by the phase angle of ~80 °C for the electrodes with less than 7.85 kμm^2 geometrical surface area. Another notable trend was that the impedance decreased with an increase in electrode area. Figure 2(b) plots the impedance and phase obtained from the electrodes when measured at 1 kHz, the frequency associated with the action potential associated with cortical neural processes. The smallest electrode (496 μm^2) had an average impedance of 675 ± 130 kΩ, which decreased to 46.5 ± 4.80 kΩ for the largest, 500 Kμm^2 area electrodes. The trend lines added to the graph show a relative linearity associated with all the electrodes.

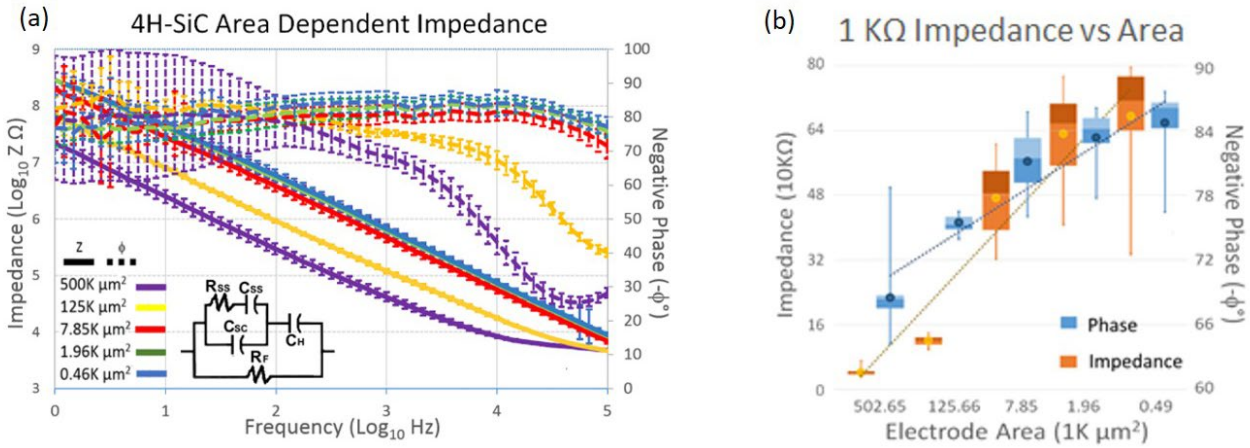

Figure 2: 4H-SiC electrode performance vs. geometrical surface area. (a) EIS data (error bars represent the standard deviation). Inset shows basic circuit model which produced an impedance profile similar to experimental data. (**b**) A box and whiskers plot for the impedance and phase at the frequency of 1 kHz vs. area. Mean impedance and phase represented with a dot. All tests performed in PBS) with a pH of 7.4.

Figure 3(a) displays select representative cyclic voltammetery, CV, curves for each of the electrodes reported in this study taken across the potential water limit for Pt (-0.6 to 0.8 V). Figure 3(b), on the other hand, shows select curves using the extended water window (-2.0 to 2.8 V) from the all-SiC electrodes. Both micrographs demonstrate a decrease in the hysteresis cycle when the area is decreased. Once again, CV data supports a dominant capacitive interaction mechanism with the electrolytic ions. The current remains constant for the CV sweep, until it nears the potential limit on either side of the test. At this point, the charge potential is reversed, leading to a large influx of current which follows the resistor-capacitor (RC) charging process. After the charging, the current once again remains constant until the next potential ramp shift.

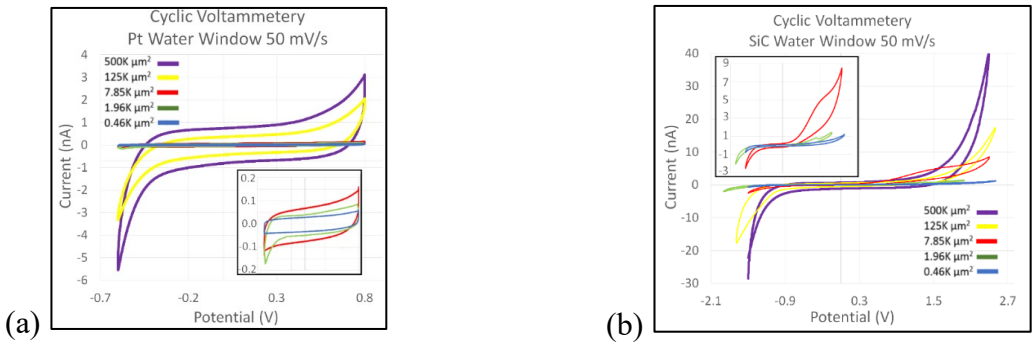

Figure 3: (a) CV plot showing a single curve from cyclic voltammetry evaluation of a select 4H-SiC electrode. Curves bounded at the potentials typically used for platinum or iridium electrodes of −0.6 V and +0.8 V. Inset shows detail for the three smallest electrodes. (b) Plot of second CV curve from a select electrode. Ramp rate same as (a), but potential limits extended until onset of a large current flux. All tests performed in 7.4 pH PBS.

3C-SiC Fabrication and Characterization: The 3C-SiC (cubic silicon carbide) all-SiC INI was developed incorporating many standard silicon semiconductor micromachining processes. This started with the epitaxial growth of a 3C-SiC film on a SOI wafer, followed by patterning of the 3C-SiC epitaxial films via thin film contact photolithography techniques. The subsequent etching of the electrode traces and recording sites used a deep-reactive ion etching (DRIE) process, followed by deposition of a conformal *a*-SiC film via PECVD, and the opening of windows in the a-SiC film via RIE (recording and wire-bonding sites). The final probe definition etch through the buried oxide layer was accomplished via additional DRIE processes. The final step was the release of the finished device from the substrate SOI wafer which was achieved through hydrofluoric acid wet etching the buried oxide layer. The fabrication steps are shown in Figure 4.

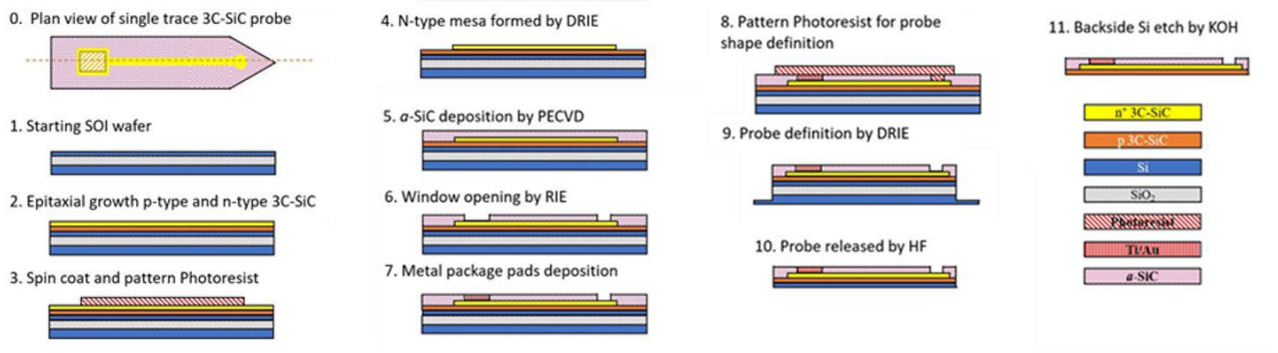

Figure 4: The fabrication flow of all-SiC neural probes. Planar MEA fabrication concluded at Step 7 for reference. Reprinted with permission from Elsevier [12].

The 3C-SiC INI were characterized using the same methods as the 4H-SiC devices. The results are presented in the summary section where comparison of all SiC neural interfaces is made. Figure 5 shows some details of the 3C-SiC devices fabricated on SOI:

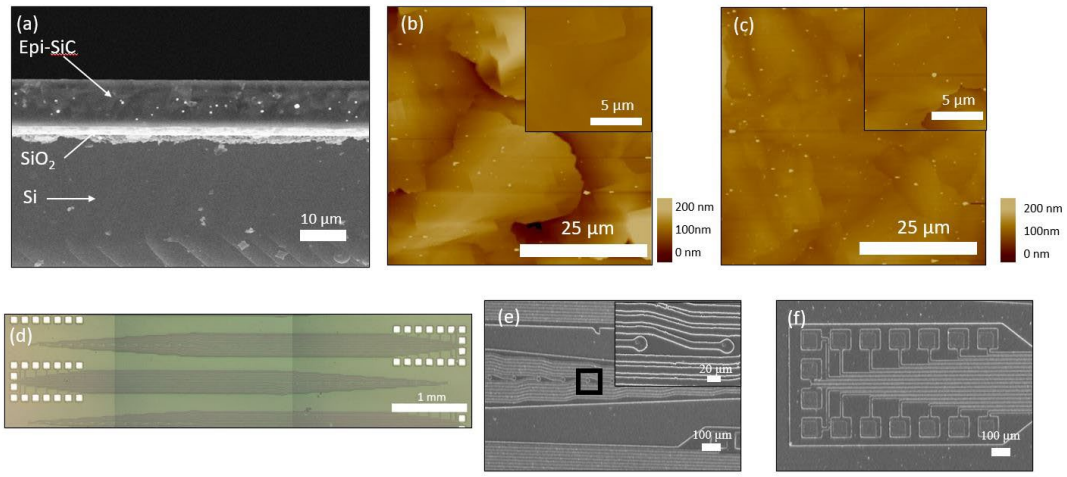

Figure 5: SEM and AFM analysis 3C-SiC films and a pre-released all-SiC neural probe. (a) Cross-section SEM micrograph of epitaxial 3C-SiC on SOI wafer. AFM analysis on the epitaxial 3C-SiC film (b) edge region of the wafer (c) center region of the wafer. (d) Optical micrograph of to be released neural probe and (e)(f) SEM micrographs of recording sites and package pads. Reprinted with permission from Elsevier [12].

Carbon-electrode SiC INI

Carbon containing materials, such as graphene, carbon-nanotubes (CNT), and graphene oxide, have gained prominence as possible electrode materials for implantable neural interfaces due to their excellent conductive properties. While carbon is a promising electrochemical interface, reliable and repeatable fabrication processes are needed for reliable and repeatable device production and this factor impacts large scale device production. Here we demonstrate that carbon (C) electrodes and traces constructed from pyrolyzed-photoresist-film (PPF), when combined with amorphous silicon carbide (*a*-SiC) insulation, can be fabricated with repeatable processes using tools easily available in most semiconductor facilities. Directly forming C on *a*-SiC simplifies the fabrication process while eliminating noble metal evaporation/sputtering and lift-off processes. C electrodes in oxygenated phosphate buffered solution at pH 7.4 demonstrated excellent electrochemical charge storage capacity (CSC) of 14.16 C/cm^2, an impedance of 24.8 ± 0.4 kΩ, and phase angle of −35.9 ± 0.6° at 1 kHz with a 1.9 Kμm^2 recording site area.

C on a-SiC Fabrication and Characterization: The C/*a*-SiC INI was fabricated via standard semiconductor micromachining processes. As reported in [10], *a*-SiC was deposited by Plasma Enhanced Chemical Vapor Deposition (PECVD) using 12 sccm SiH_4 and 360 sccm CH_4 as silicon and carbon precursors along with 700 sccm Ar carrier gas. The chamber was heated to 250 °C, pressure maintained at 1100 mTorr, and an RF plasma was applied with a power of 200 W. Positive

photoresist (AZ12xt) was spin-coated at 500 rpm for 20 s, 3000 rpm for 50 s, and 11,000 rpm for 2 s for a ~7 µm layer measured via stylus profilometer on the surface of the deposited a-SiC. The resist coated substrate was soft-baked at 120 °C for 3 min which was then followed by UV exposure at 120 mJ/cm^2. Next, a one-minute post-exposure bake at 95 °C was performed and followed by pyrolyzation within a 900 °C annealing tube furnace held at atmospheric pressure under an Ar and H_2 environment of 100 sccm and 5 sccm, respectively. Thermal ramp rate was 10 °C/min, followed by a thermal soak at 900 °C for one hour. After annealing, the wafer was cooled down to room temperature while remaining under the same flow of Ar and H_2. The top, conformal *a*-SiC insulator layer was then deposited on the pyrolyzed C layer as per the base layer process. Contact and electrode windows were opened in the top insulator through reactive ion etching (RIE) for 5 minutes time: 37 sccm CF_4 and 13 sccm O_2, RF power 200 W, and a base pressure of 50 mTorr. Bond pads were formed on the contact mesas via E-beam evaporation starting with 50 nm of Ti as an adhesion layer followed by 300 nm of Au to facilitate device packaging. The die was then bonded to a Si handle wafer device side down using crystal bond (Ted Pella, Inc.) and the silicon substrate was thinned using deep reactive ion etching (DRIE) to achieve a 50 µm Si supporting layer. The final process step was to harvest the probes from the Si handle wafer via dissolution of the crystal bond adhesion layer in acetone. The C sandwiched with *a*-SiC was characterized for both its material and electrical properties as shown in Figure 6 below. Resistivity measurement was performed using the double-ended resistors from the planar MEA of Figure 1. The resistivity was ~3 mΩ-cm for a C film thickness of 387 nm and a trace width of 10 µm.

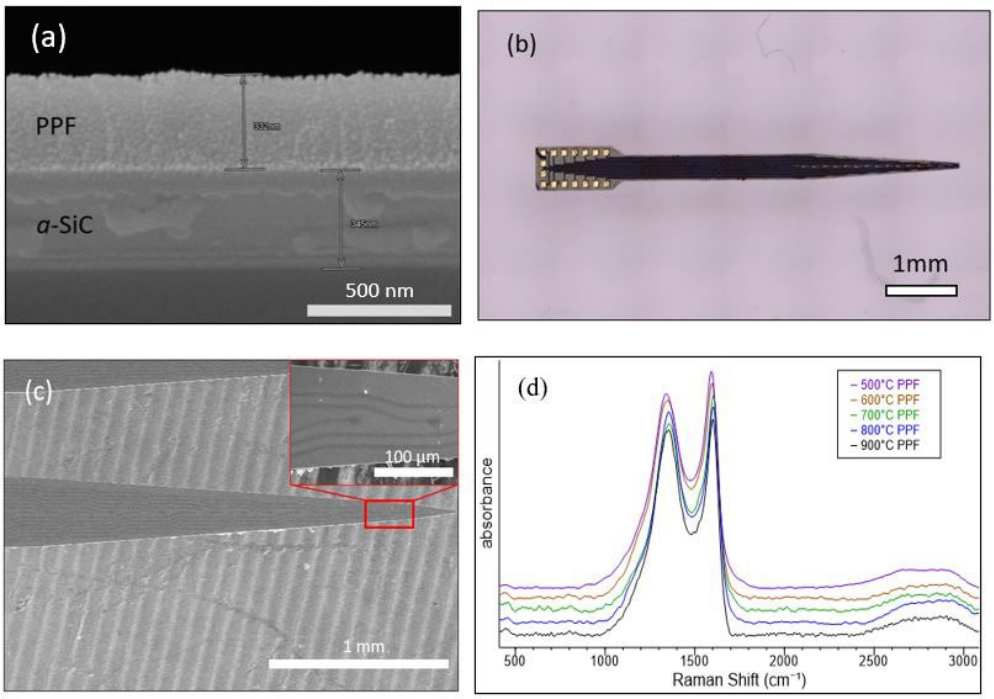

Figure 6: Fabricated C on *a*-SiC probe characterization data: (a) SEM cross section micrograph after PPF annealing at 900°C. Photoresist thickness 7.4 µm prior to annealing and of 387 nm after annealing (~ 92% vertical shrinkage). (b) Composite optical image of single shank *a*-SiC/C neural probe. (c) SEM plan view micrograph showing electrode and recording tip detail. (d) Raman Spectra of C films on *a*-SiC versus annealing temperature shows a 10 cm^{-1} red shift with increasing annealing temperature indicating improved PPF film structure. Reprinted with permission from Micromachines [10].

Electrochemical characterization was performed using the identical methods as the 4H- and 3C-SiC INI. This time comparison with a standard Pt metal electrode was performed in order to baseline the C/*a*-SiC probe performance to a known standard.

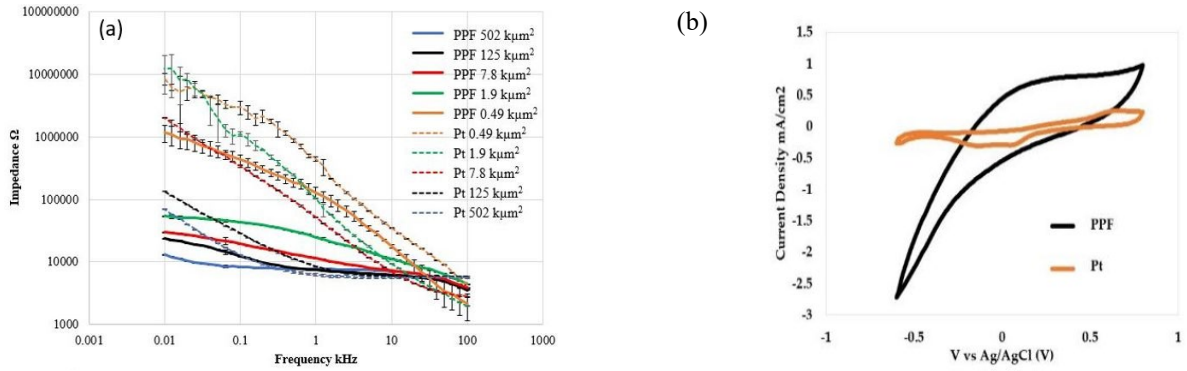

Figure 7: Electrochemical performance of C/*a*-SiC and Pt reference electrode. (a) PPF (C) and Pt EIS impedance vs. frequency and (b) CV data comparison of PPF (C) (900°C) vs. Pt with same recording area (502 kμm^2). Note significantly larger curve area for PPF vs. Pt indicating superior charge storage capacity. Reprinted with permission from Micromachines [10].

MRI Performance of 3C-SiC Neural Interfaces

This last section looks at the magnetic resonance imaging (MRI) compliance of cubic silicon carbide (3C-SiC) INI through finite element method (FEM) simulations followed by device exposure to 7 Tesla MRI fields while placed within a brain tissue phantom. The simulations were used to predict induced tissue heating as well as static magnetic field ($\mathbf{B_0}$) perturbation to understand image artifact generation, and the MRI experiments to validate the simulation results. The MRI safety of 3C-SiC is compared to other materials commonly used for neural implants such as platinum (Pt) and silicon (Si). The outcome is a comparative study with respect to MRI-induced $\mathbf{B_0}$ perturbation or image artifacts, and MRI-induced heating is presented to compare the MRI safety of 3C-SiC neural implants to the other materials. Results indicate that further development of an all-SiC INI constructed of 3C-SiC and *a*-SiC is warranted.

3C-SiC Neural Probe Fabrication and Characterization: As described throughout we developed monolithic planar INI fabricated from cubic silicon carbide (3C-SiC) which contained no other material, except gold (Au) which was placed on the contact pads to facilitate wire bonding to the package. This fabrication method can potentially reduce induced current in the electrode which leads to tissue heating and image artifacts. The high thermal conductivity of 3C-SiC (3.6-3.7 W/cm-K for SiC on par with pure copper (~ 3.8 W/cm-K), allows for better heat dissipation especially when compared to Si (1.49 W/cm-K). SiC possesses a magnetic susceptibility of -12.87 ppm, a factor that is much closer to brain tissue (χ = -9.05 ppm) when compared to Si (χ = -4.2 ppm). Thus, SiC has an intrinsic MRI compatibility advantage over conventional probe materials. When one considers the ability to form relatively high-resistivity conductive traces, in comparison with metals, neural probes fabricated monolithically from 3C-SiC possesses a resistance to magnetic perturbation caused by magnetic susceptibility differences and decrease the heat generated by MRI induced currents on the neural probe conductive traces.

Details of the data presented here may be found in Beygi *et Al*. [11]. Figure 8 shows a portion of the experimental data whereby an all-SiC neural probe displayed negligible image artifacts in a brain tissue phantom at 7 Tesla within an animal bore MRI system at the Moffit Cancer Center, Tampa, FL. Not shown are induced heating simulations which indicate that 3C-SiC is predicted to have a SAR value ~30% lower than Pt and below the limit established by the FDA.

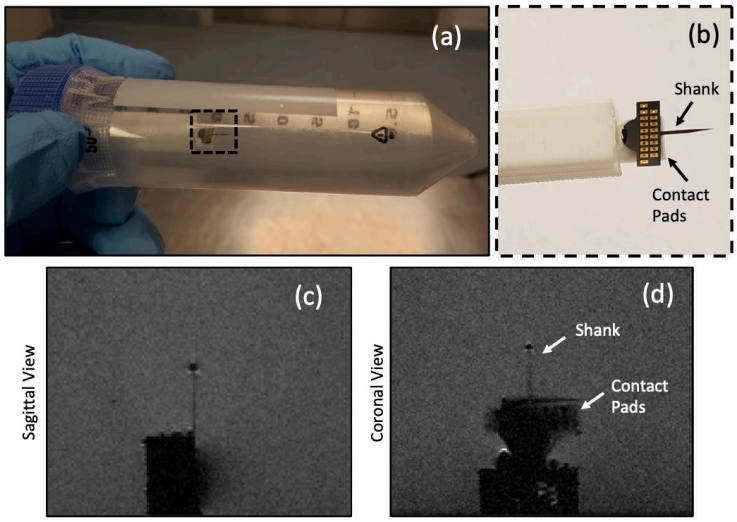

Figure 7: MRI data from a fabricated 3C-SiC all-SiC neural probe under 7 T MRI scanning. The same MRI sequence used for image artifact numerical analysis was used in this experiment. (a) Photograph of experimental setup (PLA holder, plastic tube, tissue phantom and neural probe). (b) A close-up image of the 3C-SiC neural probe glued on the PLA holder. (c) sagittal view of the neural probe under 7 T MRI. The tip of the probe showed a circular image artifact. (d) coronal view of the neural probe. The shank generated less image artifacts than the pads, due to the metallic pads which would be outside of the brain during probe use and is not an issue. Reprinted with permission from Micromachines [11].

Summary

The development of SiC-based neural interfaces has been presented with measured electrochemical performance superior to that of standard Pt electrodes. 4H- and 3C-SiC "all-SiC" monolithic neural interfaces, as well as C derived from pyrolyzed photo resist (PPF) sandwiched with *a*-SiC, were used to create these interfaces. Consequently, no metals or polymers are in contact with brain tissue which is highly significant since this is known to negatively impact long-term in-vivo reliability and performance. Table 1 provides a comparison between the results summarized here and contemporary neural interfaces showing the exceptional performance of our SiC neural interfaces.

Table 1: Electrochemical properties of SiC and common neural electrode materials.

Material	Recording area (kμm^2)	Impedance @1kHz (kΩ)	Charge storage capacity* (mC/cm^2)
4H-SiC [4]	496	375	11
3C-SiC [12]	1.9	165	74
C/*a*-SiC [10]	1.9	25	14,160
Pt [10]	1.9	104	12
PEDOT/CNT [13]	2.83	15	6
Carbon-nanotube fiber [14]	1.450	141	372
Graphene Fiber [15]	0.749	38	798
IrO_x [16]	0.177	133	29
TiN [13]	2.83	55	5

* Charge Storage Capacity (CSC) value sum of anodic and cathodic phases.

In addition to the electrochemical performance of SiC neural interfaces, a preliminary study (numerical and experimental) of the MRI compatibility of the 3C-SiC all-SiC neural interface showed very promising performance in a 7 T animal bore MRI tool indicating that the present limit of 3 T, which greatly reduces image resolution, may be exceeded. In all cases additional research is planned in animal models (rodent) to further demonstrate the utility of SiC neural interfaces for long-term human implant applications.

References

[1] Saddow, S. E., Frewin, C. L., Coletti, C., Schettini, N., Weeber, E., Oliveros, A., & Jarosezski, M. (2011). Single-crystal silicon carbide: A biocompatible and hemocompatible semiconductor for advanced biomedical applications. *Materials Science Forum* (Vol. 679, pp. 824-830). Trans Tech Publications Ltd.
[2] Saddow, S. E., *Silicon Carbide Biotechnology: A Biocompatible Semiconductor for AdvancedBiomedical Devices and Applications*. Netherlands: © 2012. Elsevier Science.
[3] Barrese, J. C., Aceros, J. & Donoghue, J. P. 2016. Scanning electron microscopy of chronically implanted intracortical microelectrode arrays in non-human primates. *J Neural Eng,* 13, 026003.
[4] Barrese, J. C., Rao, N., Paroo, K., Triebwasser, C., Vargas-Irwin, C., Franquemont, L. & Donoghue, J. P. 2013. Failure mode analysis of silicon-based intracortical microelectrode arrays in non-human primates. *J Neural Eng,* 10, 066014.
[5] Prasad, A., Xue, Q. S., Sankar, V., Nishida, T., Shaw, G., Streit, W. J. & Sanchez, J. C. 2012. Comprehensive characterization and failure modes of tungsten microwire arrays in chronic neural implants. *J Neural Eng,* 9, 056015.
[6] Grill, W. M., Norman, S. E. & Bellamkonda, R. V. 2009. Implanted neural interfaces: biochallenges and engineered solutions. *Annual Review of Biomedical Engineering,* 11, 1-24.
[7] Saddow, S. E., *Silicon Carbide Biotechnology: A Biocompatible Semiconductor for Advanced Biomedical Devices and Applications*. Second Edition. Netherlands: © 2016 Elsevier Science.
[8] Bernardin, E.K.; Frewin, C.L.; Everly, R.; Ul Hassan, J.; Saddow, S.E. Demonstration of a Robust All-Silicon-Carbide Intracortical Neural Interface. *Micromachines* 2018, 9, 412. https://doi.org/10.3390/mi9080412.
[9] Beygi, M.; Bentley, J.T.; Frewin, C.L.; Kuliasha, C.A.; Takshi, A.; Bernardin, E.K.; La Via, F.; Saddow, S.E. Fabrication of a Monolithic Implantable Neural Interface from Cubic Silicon Carbide. *Micromachines* 2019, 10, 430. https://doi.org/10.3390/mi10070430.
[10] Feng, C.; Frewin, C.L.; Tanjil, M.R.-E.; Everly, R.; Bieber, J.; Kumar, A.; Wang, M.C.; Saddow, S.E., "A Flexible *a*-SiC-Based Neural Interface Utilizing Pyrolyzed-Photoresist Film (C) Active Sites," *Micromachines* 2021,
12, 821. https://doi.org/10.3390/mi12070821.
[11] Beygi, M.; Dominguez-Viqueira, W.; Feng, C.; Mumcu, G.; Frewin, C.L.; La Via, F.; Saddow, S.E., "Silicon Carbide and MRI: Towards Developing a MRI Safe Neural Interface," *Micromachines* 2021, 12, 126.
https://doi.org/10.3390/mi12020126.
[12] Saddow, S. E., *Silicon Carbide for Medical Devices*. Netherlands: Elsevier Science, in-press (2022).
[13] Gerwig, R.; Fuchsberger, K.; Schroeppel, B.; Link, G.S.; Heusel, G.; Kraushaar, U.; Schuhmann, W.; Stett, A.; Stelzle, M. PEDOT- CNT composite microelectrodes for recording and electrostimulation applications: Fabrication, morphology, and electrical properties. *Front. Neuroeng*. 2012, 5.
[14] Vitale, F.; Summerson, S.R.; Aazhang, B.; Kemere, C.; Pasquali, M. Neural stimulation and recording with bidirectional, soft carbon nanotube fiber microelectrodes. *ACS Nano* 2015, 9, 4465–4474.
[15] Wang, K.; Frewin, C.L.; Esrafilzadeh, D.; Yu, C.; Wang, C.; Pancrazio, J.J.; Romero-Ortega, M.; Jalili, R.; Wallace, G. High- Performance Graphene-Fiber-Based Neural Recording Microelectrodes. *Adv. Mater*. 2019, 31, 1805867.
[16] Wilks, S. Poly(3,4-ethylene dioxythiophene) (PEDOT) as a micro-neural interface material for electrostimulation. *Front. Neuroeng*. 2009, 2, 7.